

Sentinel-1A

Radiometric Consistency between TOPS SLC and GRD Products

UZH-S1-TOPS-RADIOMETRY-TN05 -- Issue 1.0 – 30.05.2016

VEGA Contract No. VEGA/AG/15/01757



Authors: Adrian Schubert & David Small
Remote Sensing Laboratories – University of Zurich, Switzerland



Distribution List	
Name	Affiliation
Nuno Miranda	ESA-ESRIN
David Small	RSL
Adrian Schubert	RSL

Document Change Record			
<i>Issue</i>	<i>Date</i>	<i>Page(s)</i>	<i>Description of the Change</i>
0.7	15.03.2016		Initial internal draft
0.9	17.03.2016		Delivery to ESA, with results from missing products be appended once the data become available
1.0	30.05.2016		Delivery to ESA, with updated results and analysis reflecting products received after the delivery of v0.9.

TABLE OF CONTENTS

1 INTRODUCTION	5
1.1 ACRONYMS	5
2 ELLIPSOID-GEOCODING.....	7
2.1 METHOD	7
2.2 DATA ACQUISITIONS.....	7
3 RADIOMETRIC COMPARISONS	8
3.1 IW ASCENDING (SWITZERLAND/FRANCE, 2016.02.20 17:31 VV)	9
3.2 IW DESCENDING (SWITZERLAND/ITALY, 2016.02.02 05:34 VV)	10
3.3 EW ASCENDING (BRAZIL, 2016.02.02 23:02 HH)	12
3.4 EW DESCENDING (GERMANY, 2015.07.13 05:34 VV).....	15
3.5 CONCLUSIONS	16
4 RECOMMENDATIONS	17
5 REFERENCES	18

LIST OF TABLES

Table 1: Document acronyms.....	5
Table 2: Sentinel-1 Product List.....	7

LIST OF FIGURES

Figure 1: IW GRD backscatter for tested products (black: -20dB, white: +5dB)	8
Figure 2: IW GRDM – MLD_SLC backscatter, Switzerland/France; histogram of differences with ~50 m samples geocoded to a 100 m grid, IPF v2.60.	9
Figure 3: IW GRDH – MLD_SLC backscatter, Switzerland/France; histogram of differences with ~50 m samples geocoded to a 100 m grid, IPF v2.60.	10
Figure 4: IW GRDM -MLD_SLC backscatter, Switzerland/Italy; histogram of differences with ~50 m samples geocoded to a 100 m grid, IPF v2.60.	11
Figure 5: IW GRDH – MLD_SLC backscatter, Switzerland/Italy; histogram of differences with ~50 m samples, 100 m grid, IPF v2.60.	12
Figure 6: EW GRDM - MLD_SLC backscatter, Brazil; same result is shown using two different colour scales to exaggerate the EW1 bias. Approximate mean dB differences are given for each beam under the images. Histogram of differences with ~80 m samples geocoded to a 0.00083333° (~90 m) grid, IPF v2.60.	13
Figure 7: EW GRDH - MLD_SLC backscatter, Brazil; histogram of differences with ~80 m samples geocoded to a 0.00083333° (~90 m) grid, IPF v2.60.	14
Figure 8: EW GRDM – MLD_SLC backscatter, Germany; same result is shown using two different colour scales to exaggerate EW1 bias. Histogram of differences with ~80 m samples geocoded to a 100 m grid, IPF v2.52.	15
Figure 9: EW GRDH – MLD_SLC backscatter, Germany; histogram of differences with ~80 m samples geocoded to a 100 m grid, IPF v2.52.	16

1 INTRODUCTION

An objective of SAR radiometric calibration is ensuring that the backscatter estimates provided in standard products are consistent in both a relative and absolute sense to independent measures of normalised radar cross section (NRCS). That allows time-series evaluation of backscatter changes over time, both using sets of data acquired with the same sensor and cross-comparisons with imagery acquired by other sensors (e.g. S1A vs. Radarsat-2, or even S1A vs. S1B, once the second unit becomes operational).

The radiometric calibration of SAR sensors depends not only on external checks (e.g. via well understood corner reflectors) but also on evaluations of possible differences between processing stages. These can potentially cause differences in the radiometric behaviour of e.g. IMP and IMS products in the case of ENVI-SAT ASAR [3], or between GRD and SLC products in the case of Sentinel-1. An earlier investigation into the radiometric consistency of S1A TOPS products [4] revealed no significant radiometric biases between SLC and GRD products.

The goal of this study was to perform similar tests as in [4], but exclusively on TOPS products, whose characteristics are described in [1]. Products from IW and EW modes were selected over four different tests sites, each having distinct characteristics that can help reveal radiometric anomalies. The product consistency was checked in the following by first ellipsoid-geocoding the GRD products to a known reference and then performing detection and multilooking on the SLC product to produce a “square pixel” resolution approximately equal to that of the GRD product. Next, the multilook-detected SLC (henceforth MLD_SLC) backscatter values were also ellipsoid geocoded to the same reference grid.

Absolute Localisation Errors (ALE) were previously reported to be very nearly the same for GRD and SLC S1IPF product-types, as reported in [5], [7] and [8]. Subsequent internal studies have continued to support the consistency of these initial estimates, although these have mainly focused on IW mode. For the purposes of the radiometric comparisons made in this study, we consider the product co-registration to be of sufficiently high quality to be excluded as a significant error source.

1.1 Acronyms

The acronyms used in this document are listed in Table 1.

Table 1: Document acronyms

ALE	Absolute Location Error
CR	Corner Reflector
DGPS	Differential GPS (Global Positioning System)
DLR	German Aerospace Centre (<i>Deutsches Zentrum für Luft- und Raumfahrt</i>)
EAP	Elevation Antenna Pattern
ESA	European Space Agency
ETRF	European Terrestrial Reference Frame
EW	Extended Wide swath mode (S1A)

FFT	Fast Fourier Transform
GNSS	Global Navigation Satellite System
GRD	Ground Range Detected
GRDF	Ground Range Detected Full-resolution
GRDH	Ground Range Detected High-resolution
GRDM	Ground Range Detected Medium-resolution
IMP	ENVISAT Imaging Mode Precision
IMS	ENVISAT Imaging Mode SLC
IOCR	In-Orbit Commissioning Review
ITRF	International Terrestrial Reference Frame
IW	Interferometric Wide swath (S1A)
LUT	Look-Up Table
MLD	Multi-Look Detected
NRCS	Normalised Radar Cross Section
OSV	Orbital State Vector (platform position and, optionally, velocity)
POEORB	Precise orbit state vectors
RESORB	Restituted orbit state vectors
RFI	Radio Frequency Interference
S1A	Sentinel-1A
S1IPF	Sentinel-1 Instrument Processing Facility
SLC	Single-Look Complex
SM	Stripmap (S1A)
SR	Slant range
SWST	Sampling Window Start Time
UZH	University of Zurich (Switzerland)
WSM	ENVISAT Wide Swath mode Medium-resolution
WSS	ENVISAT Wide Swath mode SLC

2 ELLIPSOID-GEOCODING

2.1 Method

The SLC image was first detected, then multi-looking was applied to all three products for a given acquisition date (SLC, GRDM and GRDH) to create images with approximately square samples roughly comparable in size. Sample ground dimensions of ~50-80 m were aimed for in all cases. This was considered to be large enough to minimise mixed pixel effects while reducing speckle. Floating point rasters holding radiometrically calibrated backscatter values were output for the respective slant and ground range products. The radiometric look-up tables (LUTs) annotated within the product were applied.

In the next step, both the GRD and MLD_SLC product were ellipsoid geocoded to a common reference geometry. Range-Doppler geolocation was applied [6], whereby external precise orbital state vectors (OSVs) were used in conjunction with ESA's EO_CFI library [2] for orbit interpolation.

2.2 Data Acquisitions

The list of products included in the investigation is provided in Table 2. The products generated using IPF v2.60 are highlighted in blue to separate them from those generated using v2.70.

Table 2: Sentinel-1 Product List

Mode/ Orbit	Product Type	Site	IPF Version	Product
IW/ASC	GRDM	CH/FR	2.70	S1A_IW_GRDM_1SDV_20160220T173117_20160220T173149_010033_00EC33_CABA.SAFE
	GRDH		2.60	S1A_IW_GRDH_1SDV_20160220T173121_20160220T173146_010033_00EC33_22CA.SAFE
	SLC		2.60	S1A_IW_SLC__1SDV_20160220T173120_20160220T173147_010033_00EC33_AA61.SAFE
IW/DSC	GRDM	CH/IT	2.70	S1A_IW_GRDM_1SDV_20160202T053448_20160202T053520_009763_00E45C_FCD5.SAFE
	GRDH		2.60	S1A_IW_GRDH_1SDV_20160202T053452_20160202T053517_009763_00E45C_F30F.SAFE
	SLC		2.60	S1A_IW_SLC__1SDV_20160202T053451_20160202T053518_009763_00E45C_6C59.SAFE
EW/ASC	GRDM	BR	2.60	S1A_EW_GRDM_1SDH_20160202T230204_20160202T230313_009773_00E4A4_E101.SAFE
	GRDH		2.60	S1A_EW_GRDH_1SDH_20160202T230204_20160202T230313_009773_00E4A4_2DD8.SAFE
	SLC		2.60	S1A_EW_SLC__1SDH_20160202T230204_20160202T230313_009773_00E4A4_DB89.SAFE
EW/DSC	GRDM	DE	2.70	S1A_EW_GRDM_1SDV_20150713T053425_20150713T053446_006788_0091FE_ADC2.SAFE
	GRDH		2.70	S1A_EW_GRDH_1SDV_20150713T053425_20150713T053446_006788_0091FE_CFab.SAFE
	SLC		2.70	S1A_EW_SLC__1SDV_20150713T053425_20150713T053446_006788_0091FE_OCA0.SAFE

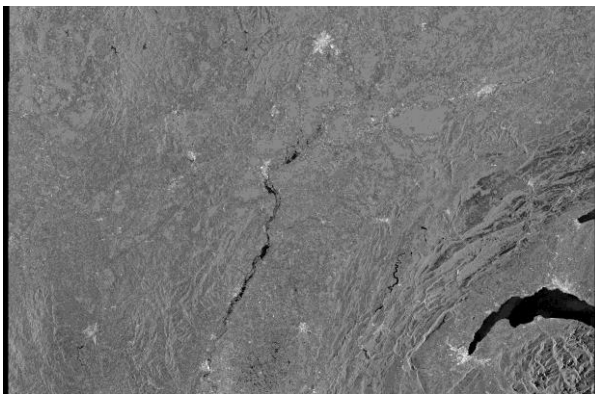
3 RADIOMETRIC COMPARISONS

Results from the radiometric comparisons between GRD and MLD_SLC ellipsoid-geocoded products are reported here.

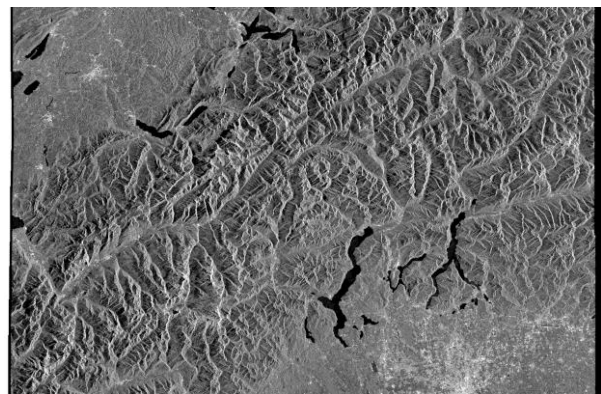
Four TOPS acquisitions were investigated: one IW ascending over Switzerland/France, one IW descending over Switzerland/Italy, one EW ascending over Brazil and one EW descending over Germany. The product types obtained were SLC, GRDH and GRDM, with SLC used as the reference for comparisons with the GRD products in each case. For all of the SLCs, an additional pre-processing step needed to be applied before ellipsoid geocoding: they were first deburstured and mosaicked into a single slant range image geometry, where detection was applied before the ellipsoid geocoding step.

In Figure 1, the GRDM gamma-nought co-polarisation backscatter is shown for each acquisition, with consistent radiometric output scaling from -20 to +5 dB. No obvious radiometric artefacts were seen in the GRDM products at this stage.

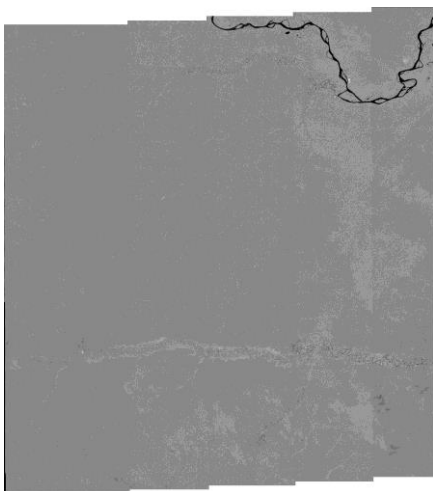
The radiometric differences between the GRD and SLC products are shown and discussed in the following sections.



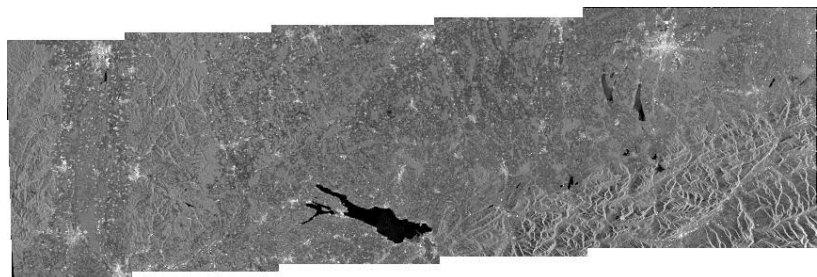
(a) IW ASC VV, Switzerland/France, 2016.02.20



(b) IW DSC VV, Switzerland/Italy, 2016.02.02



(c) EW ASC HH, Brazil, 2016.02.02



(d) EW DSC VV, Germany, 2015.07.13

Figure 1: IW GRD backscatter for tested products (black: -20dB, white: +5dB)

3.1 IW Ascending (Switzerland/France, 2016.02.20 17:31 VV)

The radiometric differences between the GRDM-MLD_SLC and the GRDH-MLD_SLC product pairs for the ascending IW acquisition over Switzerland/France are shown in Figure 2 and Figure 3, scaled between -6dB and +6dB.

No obvious regional biases are visible, with the mean absolute difference < 1 dB in both cases. There is a slight positive bias over Lake Geneva in the south-eastern image corner. This may reflect slightly different treatment of dark areas near the noise floor in the IPF routines generating the GRD and SLC products.

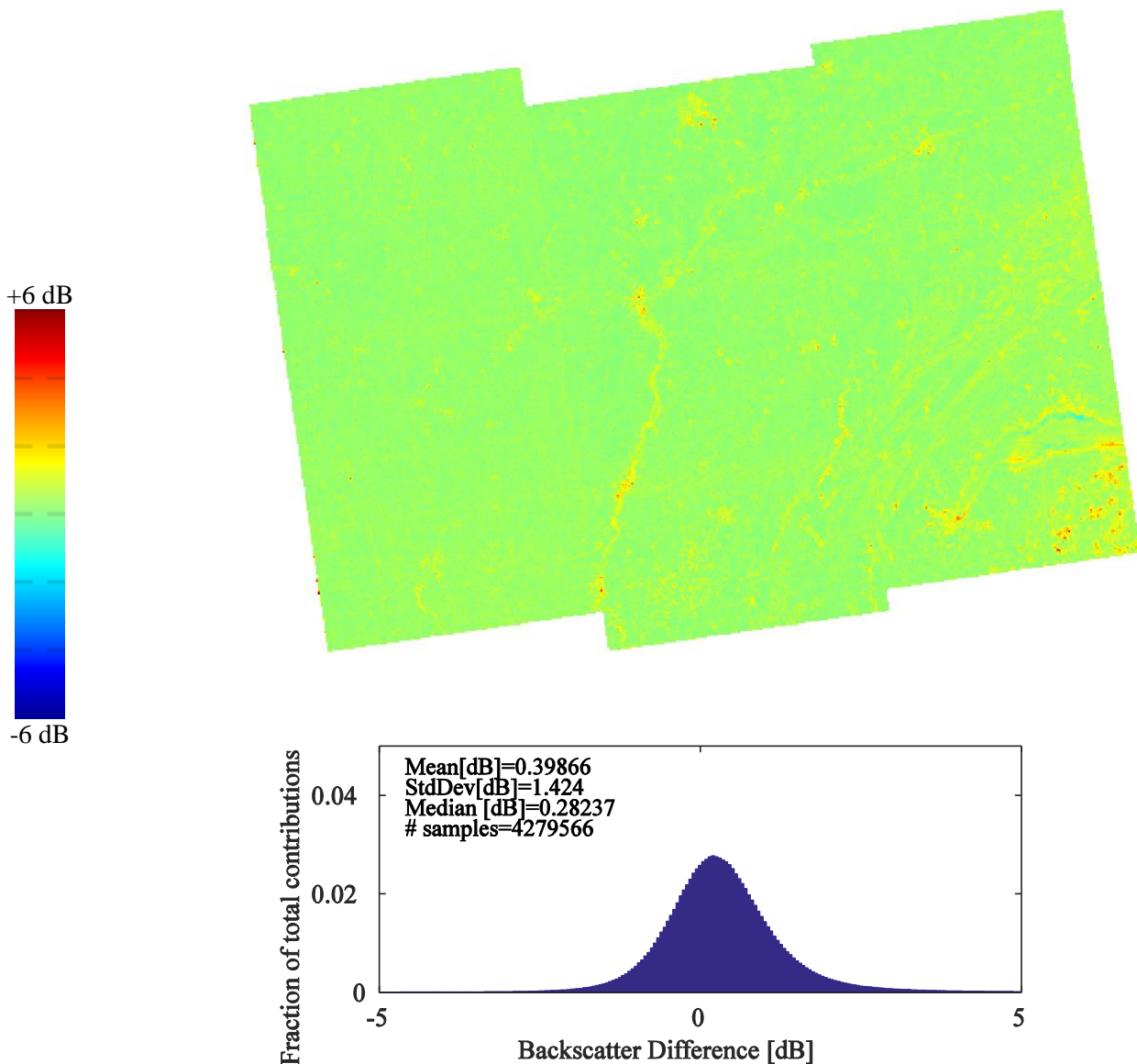


Figure 2: IW GRDM – MLD_SLC backscatter, Switzerland/France; histogram of differences with ~50 m samples geocoded to a 100 m grid, IPF v2.60.

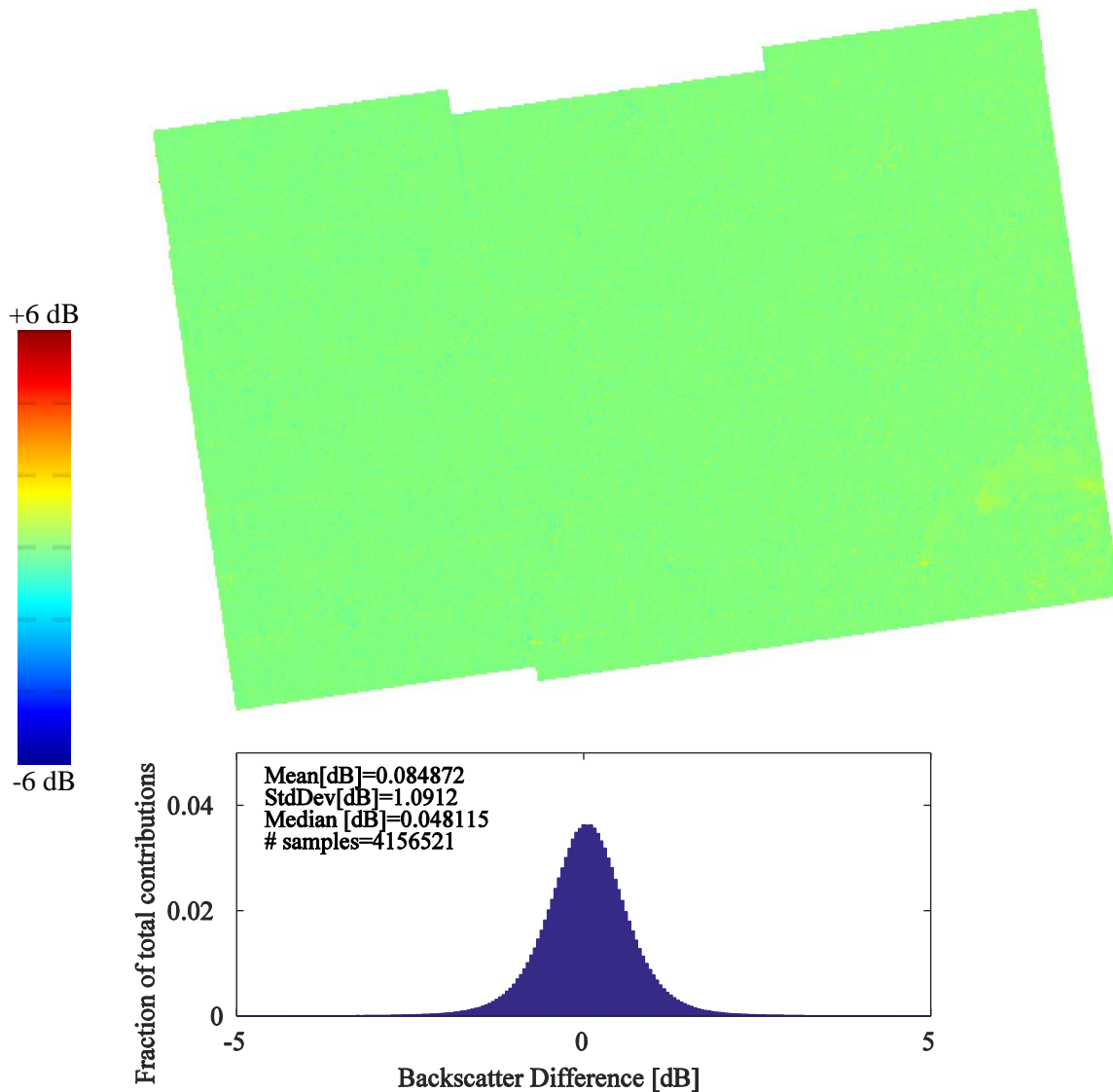


Figure 3: IW GRDH – MLD_SLC backscatter, Switzerland/France; histogram of differences with ~50 m samples geocoded to a 100 m grid, IPF v2.60.

Another effect that can be observed, more clearly in the GRDM-SLC comparison in Figure 2, is “high frequency noise” visible as yellowish, linear “strands” that follow mainly high contrast features. This can be explained by considering the different *native* product resolutions (GRDM: 40x40 m; GRDH: 10x10 m; SLC: ~14 m azimuth x ~2.3 m range), in combination with the imperfect product grid alignments caused by using integral multi-looking factors that produce slightly different ground sample spacings (prior to the geocoding step). Such effects are mainly visible in areas of steep topography and sharp contrasts and do not necessarily reflect actual radiometric product differences.

3.2 IW Descending (Switzerland/Italy, 2016.02.02 05:34 VV)

Figure 4 and Figure 5 show the GRD vs. MLD_SLC radiometric comparisons for an IW acquisition from a descending orbit over Switzerland/Italy.

The “high frequency noise” effect previously observed in Figure 2 can be seen even more clearly in the GRDM-SLC comparison in Figure 4, present mainly over the Alpine terrain that dominates this acquisition.

As before, this is best understood by considering the different native product resolutions, in combination with the imperfect alignment of the product grid spacings. Such effects are mainly visible over regions of rapid topographical variation, and do not necessarily reflect actual radiometric product differences.

No large regional differences were observed, although some minor systematic biases were seen along the sub-swath boundaries in the GRDH-SLC comparison shown in Figure 5. This was likely due to differing sub-swath merging rules being applied during generation of the GRDH product and the SLC-mosaicking applied at UZH. The histograms shown below the difference images both indicate a mean of < 1 dB, as for the ascending IW product comparisons in the previous section.

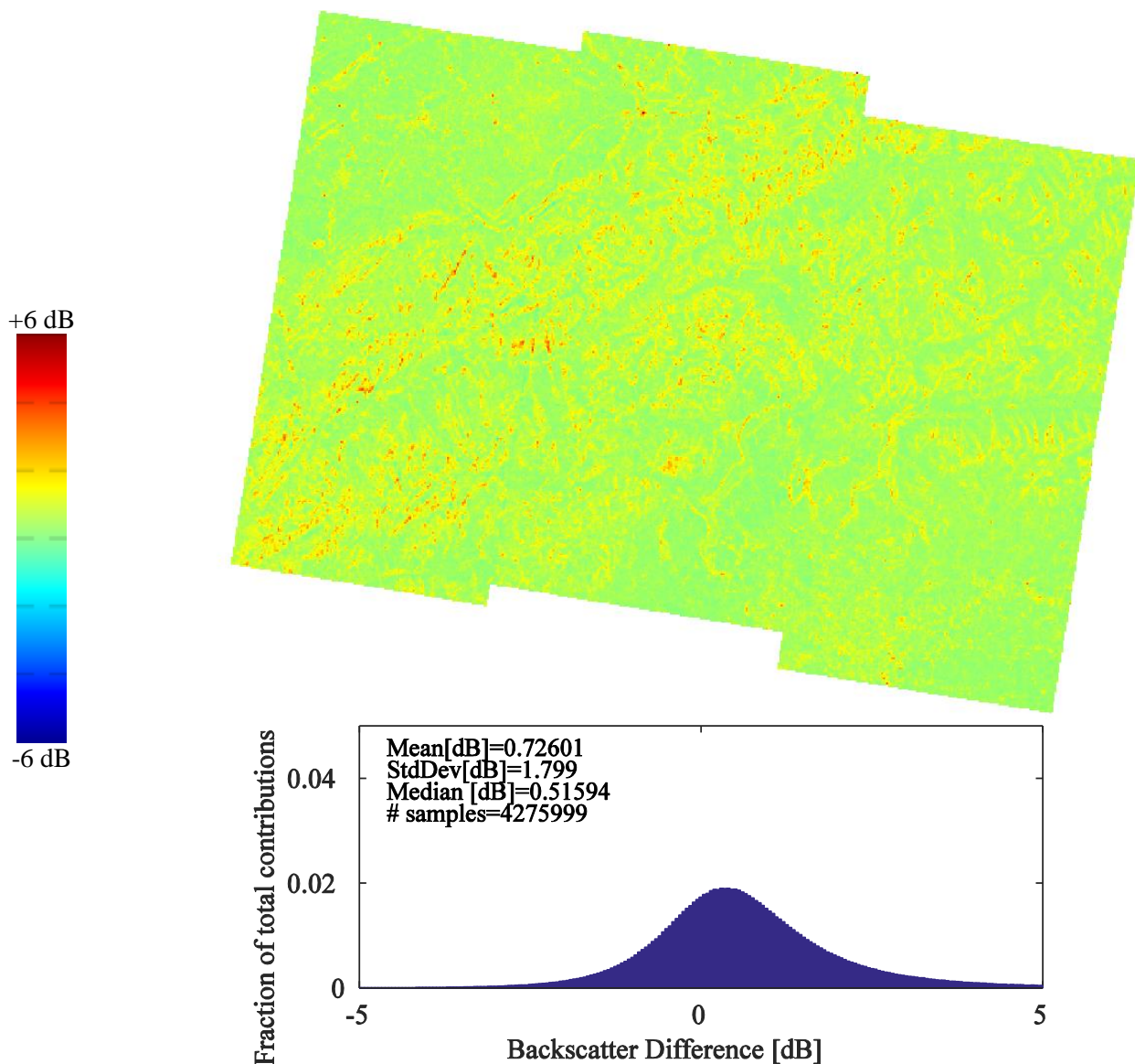


Figure 4: IW GRDM -MLD_ SLC backscatter, Switzerland/Italy; histogram of differences with ~50 m samples geocoded to a 100 m grid, IPF v2.60.

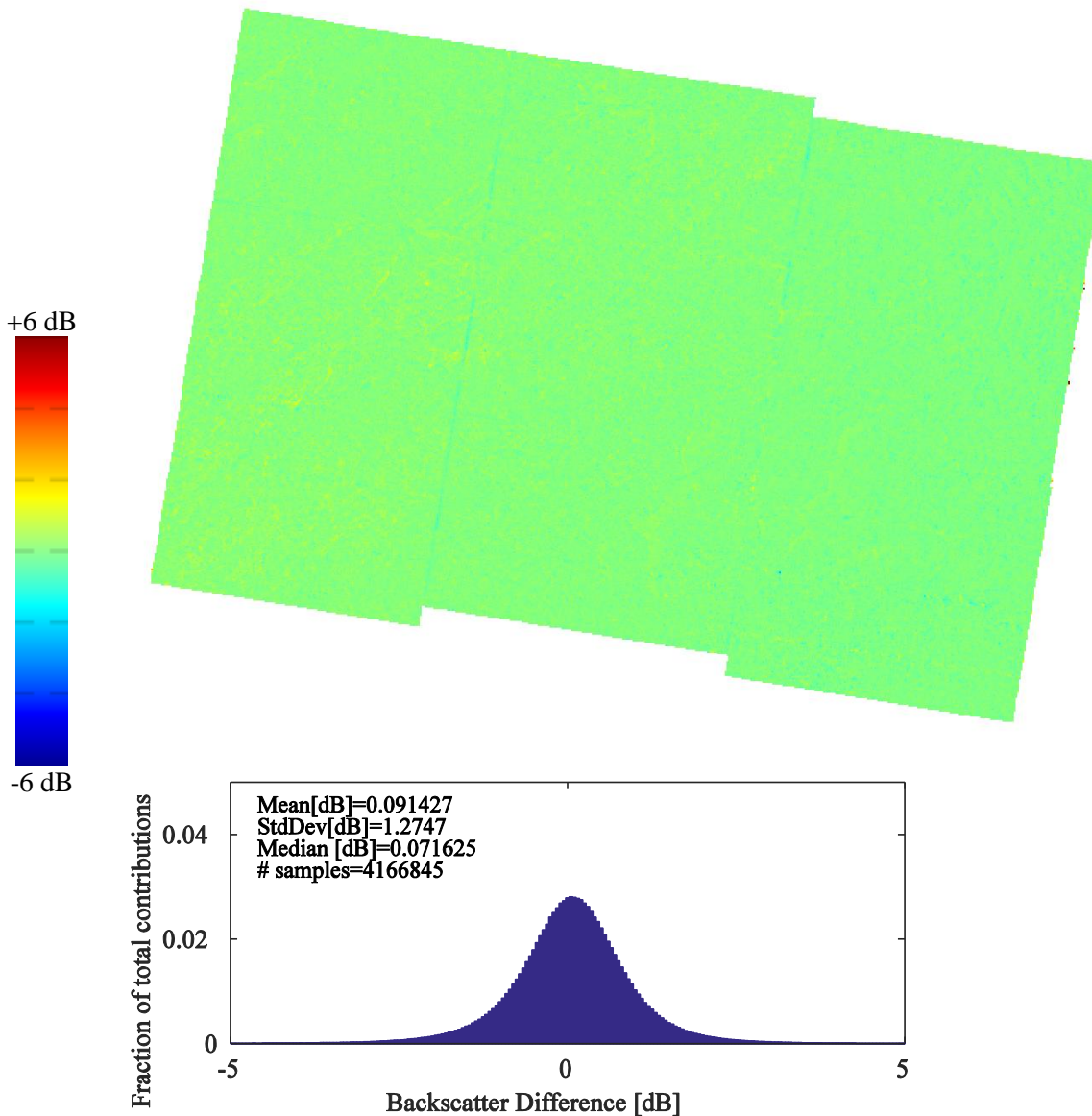


Figure 5: IW GRDH – MLD_SLC backscatter, Switzerland/Italy; histogram of differences with ~50 m samples, 100 m grid, IPF v2.60.

3.3 EW Ascending (Brazil, 2016.02.02 23:02 HH)

An acquisition over the western Brazilian rainforest was analysed, where the backscatter characteristics are well understood and the relative lack of features makes it possible to observe radiometric variations without interference from e.g. steep topography. The GRDM-MLD_SLC and GRDH-MLD_SLC differences are shown in Figure 6 and Figure 7. The differences are shown twice in Figure 6, once with radiometric scaling from -6 to +6 dB as everywhere else in this report, and once with a scale of -0.5 to +0.5 dB to exaggerate the visibility of the beam-dependent effects.

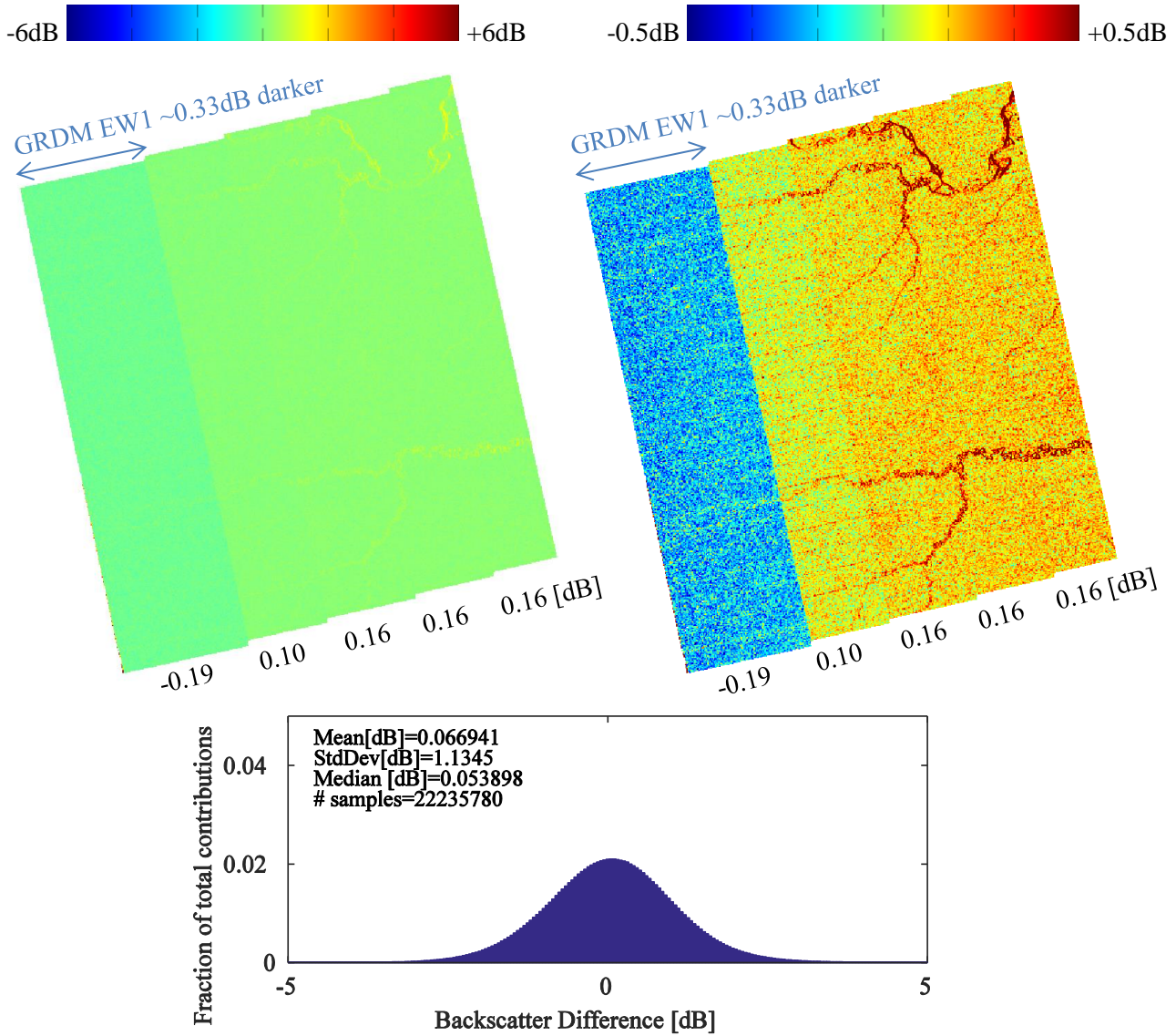


Figure 6: EW GRDM - MLD_SLC backscatter, Brazil; same result is shown using two different colour scales to exaggerate the EW1 bias. Approximate mean dB differences are given for each beam under the images. Histogram of differences with ~80 m samples geocoded to a 0.00083333° (~90 m) grid, IPF v2.60.

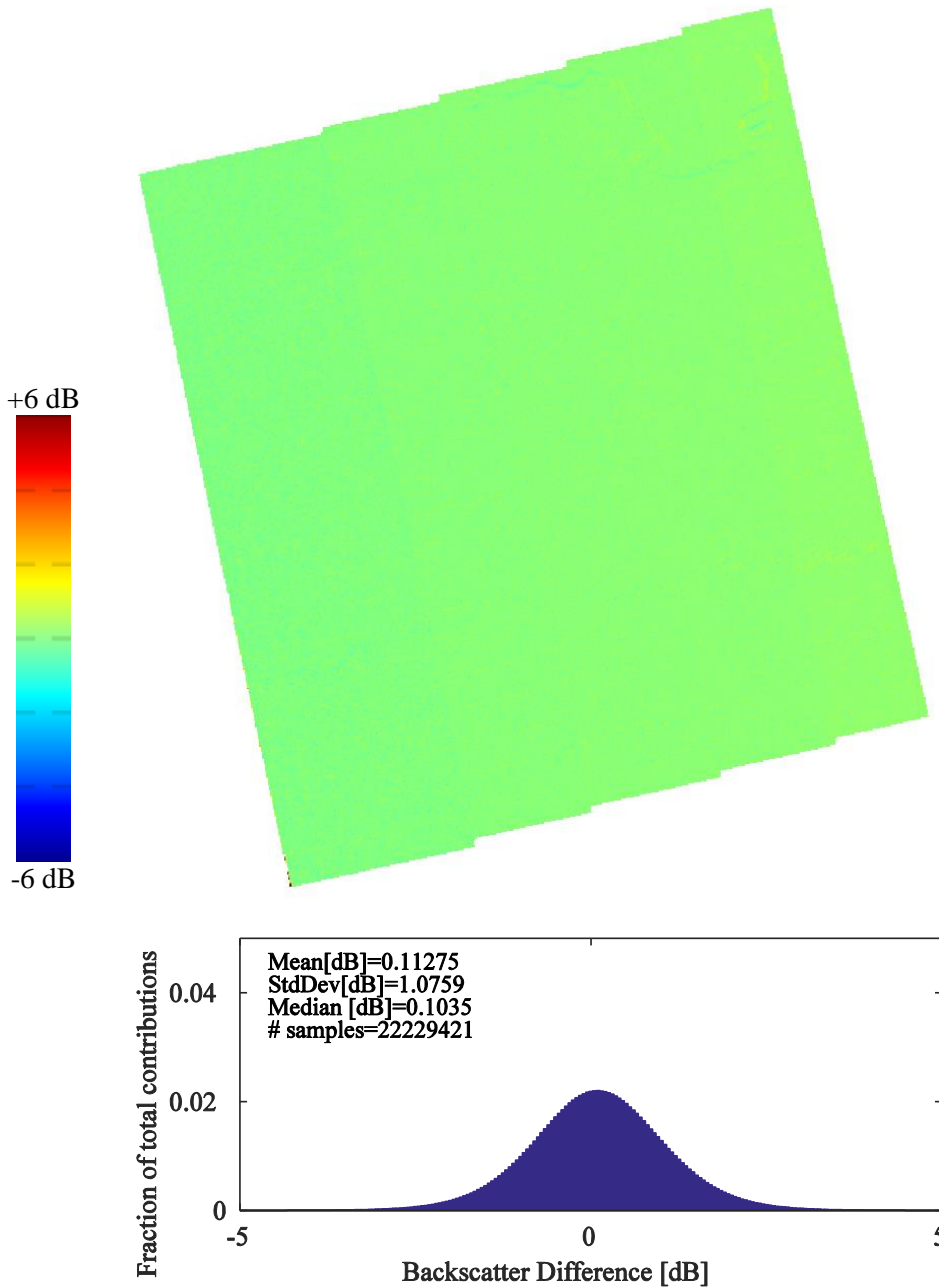


Figure 7: EW GRDH - MLD_SLC backscatter, Brazil; histogram of differences with ~80 m samples geocoded to a 0.00083333° (~90 m) grid, IPF v2.60.

The most significant feature for this acquisition is visible in Figure 6: subswath EW1 is noticeably darker than the other subswaths. The effect is shown in exaggerated form in the right-most difference image, which is more narrowly scaled. When the mean difference is estimated for each subswath separately, it becomes apparent that in fact, the subswath radiometrically most similar to the SLC is EW2. Subswaths EW3-5 are ~0.16 dB brighter. It is worth noting that the GRDM product for this acquisition was the only one generated using IPF v2.60; all other GRDM products considered were generated with IPF 2.70. These biases may reflect an error in the standard calibration normalisation as applied by these IPF versions. Note that a similar

effect is seen in the descending EW product shown in the next section, although for subswath EW4 instead of EW1.

Finally, as was seen for the area over Lake Geneva in section 3.1, the water-covered areas (rivers in this case) near the noise floor are slightly over- or under-estimated relative to the SLC product.

3.4 EW Descending (Germany, 2015.07.13 05:34 VV)

In Figure 8, the difference between an EW GRDM and corresponding MLD_SLC is shown for the descending EW acquisition over Germany. As seen in previous product comparisons, small radiometric differences connected with water bodies and steep terrain contours are visible.

However, another subtle effect visible in Figure 8 is a slight miscalibration between the subswaths, in particular EW4. This is similar to the EW1 bias seen in Figure 6, but not as strong (EW4 is only ~0.2 dB lower than the other beams). Nonetheless, it suggests a slight miscalibration of the EW GRDM subswaths.

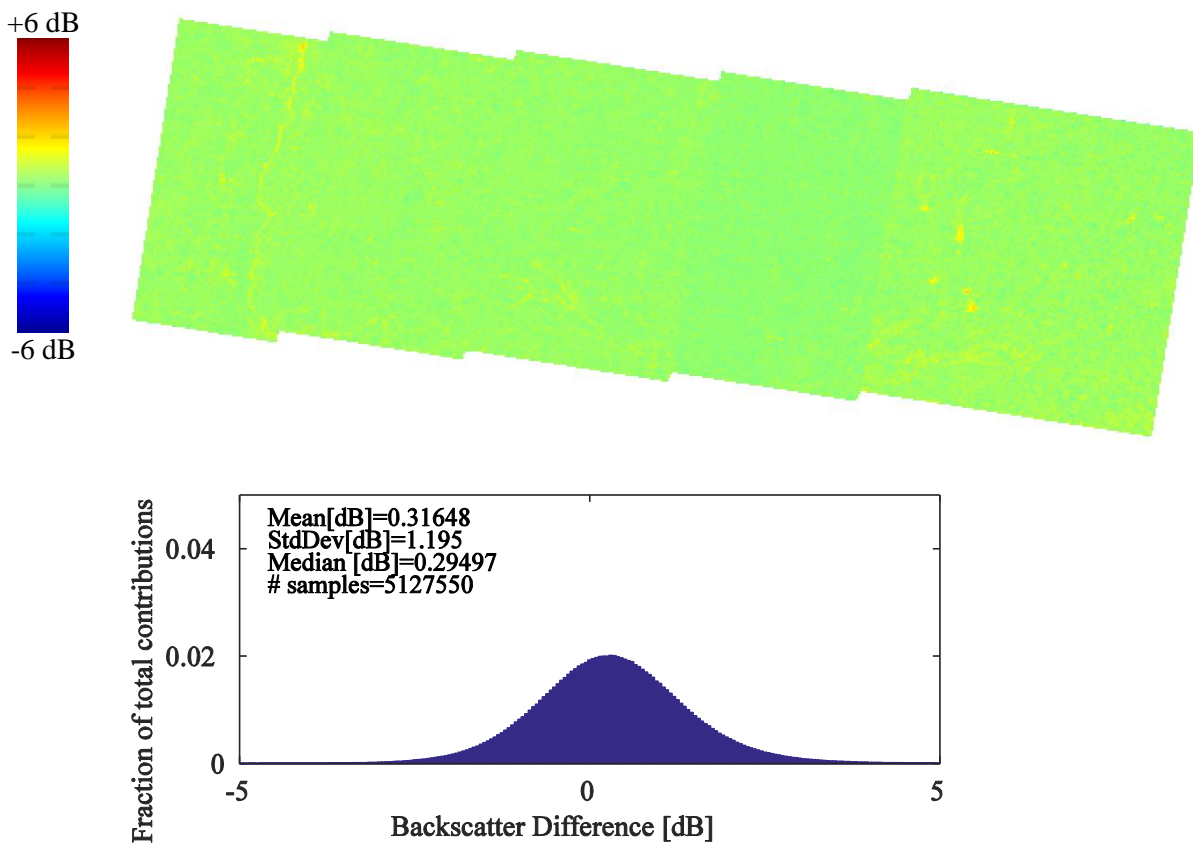


Figure 8: EW GRDM – MLD_SLC backscatter, Germany; same result is shown using two different colour scales to exaggerate EW1 bias. Histogram of differences with ~80 m samples geocoded to a 100 m grid, IPF v2.52.

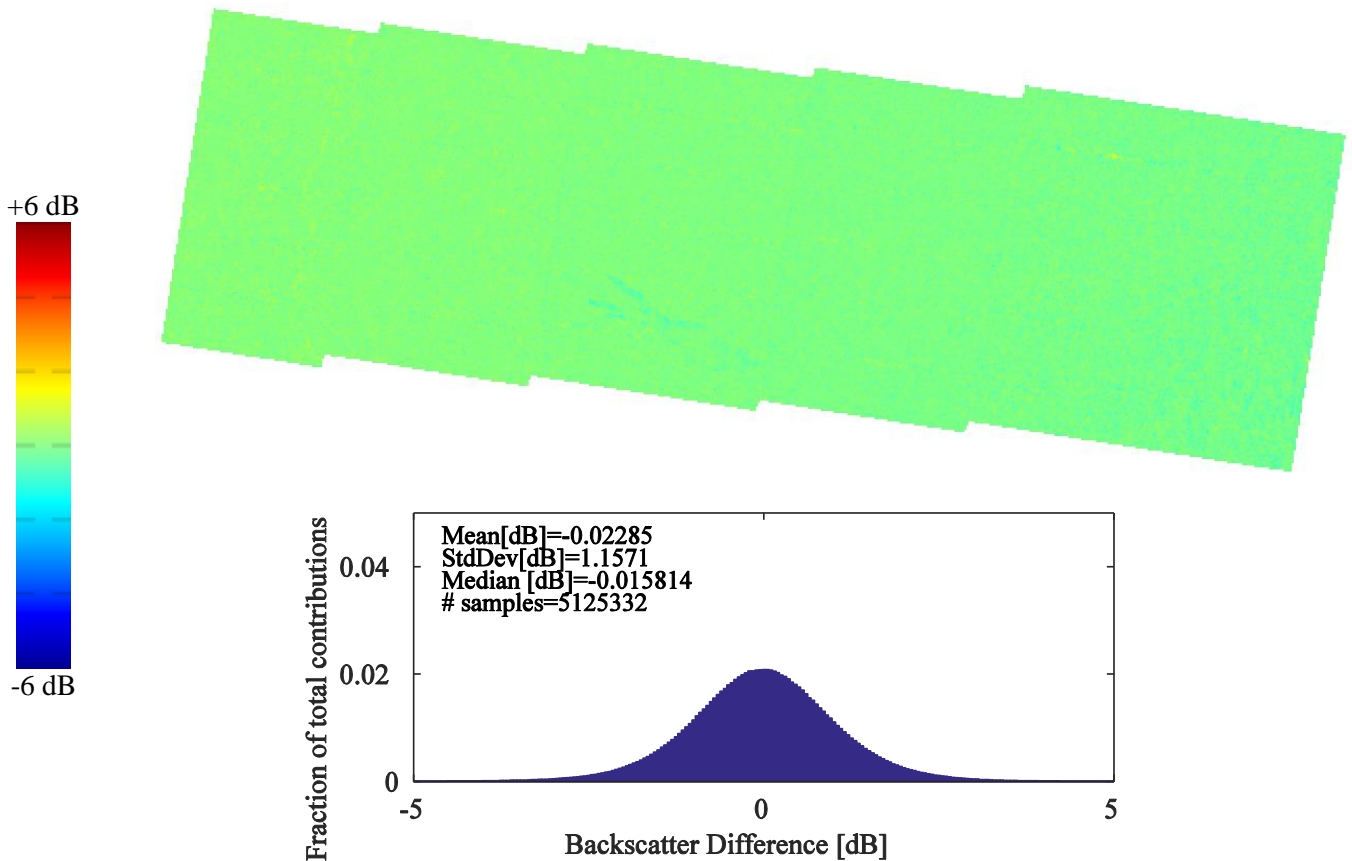


Figure 9: EW GRDH – MLD_SLC backscatter, Germany; histogram of differences with ~80 m samples geocoded to a 100 m grid, IPF v2.52.

3.5 Conclusions

For IW mode acquisitions, no large systematic differences were observed between the radiometrically calibrated SLC and GRD products investigated.

The small GRD/SLC differences that were observed could be explained by

- different product resolutions and spacings (causing small artefacts in the difference images)
- slightly different treatment of product radiometry for regions near the noise floor, such as water bodies
- possible inter-subswath miscalibration occurring in the IPF under certain conditions
- (possibly) different subswath merging algorithms at UZH (SLC mosaicking) and the IPF

EW mode GRDM products appear to have small subswath biases of approximately -0.2 dB (EW1) and +0.2 dB (EW3-5) compared with the others, which was observed in both products investigated. The same effect was seen for products generated using IPF v2.60 as with the more recent IPF v2.70.

The debursting methodology used during GRD product generation should be documented sufficiently clearly to allow closer parameterisations and duplication of the pixel boundaries when required.

Normalisation differences between realisations of the IPF when applied to SLC vs. GRD products should be tested and improved where possible.

4 RECOMMENDATIONS

The following recommendations are made:

- For EW GRDM products, the cause of the small radiometric biases observed in subswaths EW1 and EW4 should be investigated and corrected: differences between the radiometric normalisation applied to GRD vs. SLC should be reduced.
- The debursting methodology used during GRD product generation should be documented sufficiently clearly to allow closer parameterisations and duplication of the results when required.

5 REFERENCES

- [1] Aulard-Macler, M. *Sentinel-1 Product Definition*. MDA Technical Note Ref. S1-RS-MDA-52-7440; MacDonald, Dettwiler and Associates (MDA): Richmond, BC, Canada, 2012.
- [2] European Space Agency. Earth Observation Mission CFI Software, Release Notes—Version 4.8. Available online: <http://eop-cfi.esa.int/> (accessed on 24 June 2015).
- [3] Schubert A., Small D., *ENVISAT ASAR IM- & AP-Product Radiometric Consistency*, RSL-ASAR-IMAP-RAD, Issue 2.0, 17 May 2010, 28 p.
- [4] Schubert A., Small D., *Sentinel-1A Radiometric Consistency between SLC and GRD Products*, UZH-ESTEC-GEOLOC-TN-03b, Issue 1.0, February 24, 2015.
- [5] Schubert A., Small D., Miranda N., Geudtner D. & Meier E., *Sentinel-1A Product Geolocation Accuracy: Commissioning Phase Results*. *Remote Sens.* 7, 9431–9449, 2015.
- [6] Small D., Schubert A., *Guide to ASAR Geocoding*; ESA-ESRIN Technical Note RSL-ASAR-GCAD, Issue 1.01; University of Zurich, Switzerland, 2008, 36p.
- [7] Small D., Schubert A., *UZH Sentinel-1A Commissioning: Geometric Calibration*, UZH-ESTEC-GEOLOC-TN-02, Issue 1.0, 9 Oct 2014, 27p.
- [8] Small D., Schubert A., *Sentinel-1A Geometric Calibration at Torny-le-Grand, Switzerland*, UZH-ESTEC-GEOLOC-TN-03a, Issue 1.01, 19 Dec 2014, 22p.